Variability of AVHRR-Derived Clear-Sky Surface Temperature over the Greenland Ice Sheet

JULIENNE STROEVE

National Snow and Ice Data Center and Cooperative Institute for Research in Environmental Sciences, University of Colorado, Boulder, Colorado

KONRAD STEFFEN

Center for the Study of Earth from Space, Cooperative Institute for Research in Environmental Sciences and Department of Geography, University of Colorado, Boulder, Colorado

(Manuscript received 25 November 1996, in final form 14 April 1997)

ABSTRACT

The Advanced Very High Resolution Radiometer is used to derive surface temperatures for one satellite pass under clear skies over the Greenland ice sheet from 1989 through 1993. The results of these temperatures are presented as monthly means, and their spatial and temporal variability are discussed. Accuracy of the dry snow surface temperatures is estimated to be better than 1 K during summer. This error is expected to increase during polar night due to problems in cloud identification. Results indicate the surface temperature of the Greenland ice sheet is strongly dominated by topography, with minimum surface temperatures associated with the high elevation regions. In the summer, maximum surface temperatures occur during July along the western coast and southern tip of the ice sheet. Minimum temperatures are found at the summit during summer and move farther north during polar night. Large interannual variability in surface temperatures occurs during winter associated with katabatic storm events. Summer temperatures show little variation, although 1992 stands out as being colder than the other years. The reason for the lower temperatures during 1992 is believed to be a result of the 1991 eruption of Mount Pinatubo.

1. Introduction

Computation of the upwelling surface longwave flux requires accurate knowledge of the surface temperature. Not only is surface temperature crucial for calculating the longwave balance, it is also an important parameter for determining the stratification of the lower troposphere and for estimating surface turbulent fluxes of latent and sensible heat. Therefore, the surface temperature must be known to an accuracy of approximately 1 K in order to estimate the outgoing longwave flux to within 5 W m^{-2} (Steffen et al. 1993).

The main difficulty in obtaining snow surface temperatures from a satellite is due to the limited knowledge of the spatial and temporal variability of atmospheric water vapor, temperature, aerosols, and the spectral characteristics of snow. Further complications result in the inability to detect clouds over snow- and ice-covered surfaces. One means to compute the surface temperature from satellite data is through the use of a radiative transfer model. This requires acquisition of all the necessary input atmospheric parameters (e.g., temperature, water vapor, ozone, and aerosol profiles) at the time and location of the measurement to be corrected. Unfortunately, information on these parameters is generally not available and remains unknown for most of the Greenland ice sheet. Profiles of atmospheric temperature and water vapor are only available from a few coastal stations around the ice sheet and from the Swiss Federal Institute of Technology (ETH) and the University of Colorado (CU) camp (69.57°N, 49.28°W) during the summers of 1990, 1991, and 1993. This field station was established by ETH in 1990 and is currently operated by CU. Because of the lack of atmospheric profile data, the use of the radiative transfer method is limited, and other methods are sought.

Alternatives to using a radiative transfer model do exist, such as the split-window technique that uses two differentially absorbing thermal infrared channels between 10 and 13 μm (McMillin 1975), and is currently used operationally by the National Oceanic and Atmospheric Administration (NOAA) in deriving sea surface temperature (SST) (McClain et al. 1985). This approach has been employed in polar regions using Advanced Very High Resolution Radiometer (AVHRR)

Corresponding author address: Dr. Julienne Stroeve, National Snow and Ice Data Center, CIRES, University of Colorado, Box 449, Boulder, CO 80309-0449.
E-mail: Stroeve@kodiak.colorado.edu

data and the two thermal channels centered at 11 and 12 μm (Key et al. 1996; Haefliger et al. 1993; Key and Haefliger 1992; Lindsay and Rothrock 1994). Using climatological rawinsonde data, AVHRR-derived surface temperatures in the Arctic using the split-window method have been given with a theoretical accuracy of 0.1 K (Key and Haefliger 1992). This accuracy is based on the regression analysis of the modeled data and does not include measurement errors. For the Greenland ice sheet, in situ radiosonde data and measured surface temperatures from the ETH/CU camp were used to derive AVHRR surface temperatures with maximum differences of $\pm$0.6 K (Haefliger et al. 1993). To obtain this model accuracy, however, required local data and seasonal variations in atmospheric conditions were found to be important. In addition, applying coefficients and data from different NOAA satellites added errors of up to 1.0 K.

The validity of the above methods also depends on the accuracy with which the snow surface emissivity can be estimated and on the atmospheric attenuation for the two channels remaining in proportion. The latter assumption can break down for atmospheres with very low water vapor concentrations since absorption by CO_2 will begin to dominate and is more absorbing at 11 μm than at 12 μm. The errors induced by changing atmospheric conditions can be remedied by the use of satellite thermal radiances measured at different viewing angles, such as from the along-track scanning radiometer (Stroeve et al. 1996). The above-mentioned studies also rely on the modeling of the snow surface emissivity according to Dozier and Warren (1982), the accuracy of which has been disputed by Salisbury et al. (1994).

This paper examines the accuracy of AVHRR-derived surface temperatures over the Greenland ice sheet using the method of Haefliger et al. (1993). Further, using 5 years of data, the spatial and temporal variations of the surface temperatures are discussed.

2. Method

a. Satellite data

Data collected globally from AVHRR are available in two formats: at 4 km the spatial resolution is called global area coverage (GAC) or at 1.1 km it is known as local area coverage (LAC). The GAC resolution is achieved by averaging four out of every five pixels, along every third scan line. As discussed in Steffen et al. (1993), there is minimal difference between using the lower GAC and higher LAC resolution AVHRR data for climate studies over the Greenland ice sheet. This is because unlike sea ice and land areas (Steffen 1995), the major surface types of the ice sheet (glacier ice, wet snow, dry snow) extend over very large distances. Therefore, the application of low-resolution satellite data is feasible for this study, and the GAC dataset was used. The *NOAA-11* GAC data was provided by the National Center for Atmospheric Research.

From 1989 through 1993, one satellite pass for each day (at approximately 1500 GMT) centered over the Greenland ice sheet was extracted and processed. To account for the geometric distortions due to the curvature of the earth and the scanning geometry, a navigation code developed by Baldwin and Emery (1993) was used. The raw counts, or digital numbers, for each pixel were converted to brightness temperatures following the procedure given in the NOAA users' guide (Kidwell 1991), including the nonlinear corrections (Rao 1993).

The detection of clouds over snow- and ice-covered surfaces using AVHRR sensors remains an active research topic (Yamanouchi and Kawaguchi 1992; Raschke et al. 1992). However, a reliable automated cloud-masking procedure over snow and ice surfaces still does not exist. In this study, thresholds based on modeled radiances were used to classify pixels as cloudy, following the basic methodology given in the CASPR (cloud and surface parameter retrieval) cloud-masking routine (Key 1996). During daylight, the difference in brightness temperatures for both thermal channels, the reflectance in the middle infrared, and the ratio of reflectance between the near-infrared and visible channels were used. The ice sheet was divided into a dry snow region and a wet snow region based on the AVHRR-measured reflectance in the near infrared.

During polar night, only the brightness temperature differences between the two thermal channels were used. The ice sheet was divided into three different regions based on the channel 4 brightness temperature: 1) $T_4 < 220$ K, 2) $220 \leq T_4 \leq 230$ K, and 3) $T_4 > 230$ K, with each region having a different threshold for the brightness temperature difference. The thresholds of the brightness temperature differences for each region were determined after a visual inspection of the data. It was found that the thresholds needed to be tuned slightly from month to month (November–March) to maximize the accuracy of the cloud detection.

Pixels were initially classified as cloudy if the values of the above cited parameters were above or below the modeled reference values. Statistics were then calculated for the potentially clear pixels, and the threshold technique was applied again to find pixels that did not fall within the mean and their standard deviations. Comparison with observational data from the ETH/CU research camp at the equilibrium line altitude along the western slope of the ice sheet (Fig. 1) show that clouds are correctly identified 86% of the time during summer. No observational data was available during polar night, but a visual inspection of image texture reveals that the algorithm is accurate about 75%–80% of the time (subjective estimate).

b. Surface temperature

Surface temperature retrieval from satellite thermal radiances requires corrections for atmospheric attenu-

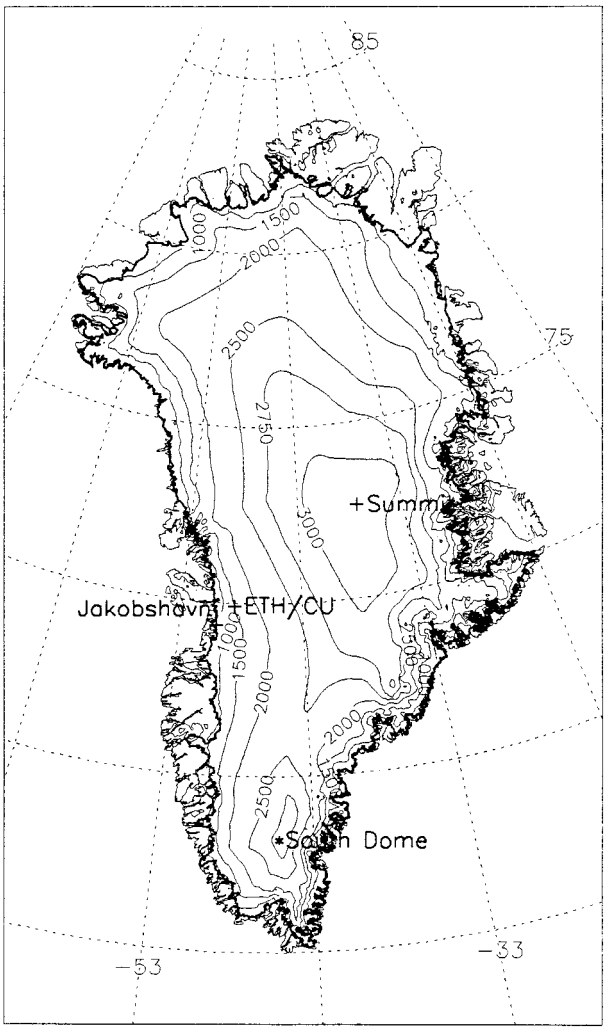

FIG. 1. Map of Greenland showing elevation contours and locations of the Summit, South Dome, Jakobshavn, and ETH/CU camp.

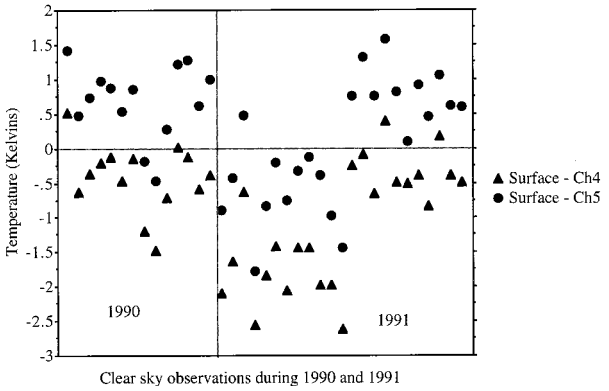

FIG. 2. Surface temperature minus coincident AVHRR GAC satellite brightness temperature for the two thermal channels (T_4 and T_5) for clear skies, measured at the ETH/CU camp during the summers of 1990 and 1991.

ation and knowledge of the surface emissivity. Although there is only minor attenuation of the surface-emitted energy in the infrared window channels by the cloud-free polar atmosphere, the difference between actual surface and AVHRR brightness temperatures can be as large as 3 K during summer (Fig. 2). The conversion from satellite brightness temperature to surface temperature can be of either sign (i.e., sometimes the surface temperature is greater than the satellite-measured temperature; sometimes the reverse is true). During winter, the atmospheric correction is much smaller due to the extremely low ($\sim$0.2 g cm^{-2}) moisture content of the winter Arctic atmosphere.

The determination of surface temperature using satellite infrared data is also limited by the variability of the surface emissivity (e.g., Price 1983). Dozier and Warren (1982) showed that the infrared emissivity of snow is primarily a function of viewing angle and not dependent upon snow properties. If this assumption is valid, then it is possible to extract snow surface temperatures using a similar methodology as for SST retrieval.

However, recent snow directional-hemispheric reflectance measurements by Salisbury et al. (1994) showed the emissivity to be dependent upon snow grain size and packing fraction, causing snow emissivity to be as low as 0.95 at 13 μm for coarse granular snow. This can result in temperature measurements at nadir to be in error by as much as 3 K (Wald 1994). With respect to the AVHRR thermal channels, using the emissivity values as given by Salisbury et al. (1994), instead of those of Dozier and Warren (1982), may result in a 0.75-K temperature difference for channel 4 and 1.32 K for channel 5. Although snow grain size and packing fraction are important, angular effects on emissivity may still dominate at the wavelengths of the AVHRR thermal channels for naturally occurring snow (Wald 1994). Failure to account for the effects of viewing angle can lead to temperature errors as large as 1.5 K for the AVHRR viewing angles.

It is very difficult to include the effects of changing grain size on snow emissivity, as information on grain size is not available on a large scale. However, due to constant wind-transported snow, it is safe to assume that the grain size remains relatively constant over most of the ice sheet during periods with no melt. Making this assumption, the algorithm of Haefliger et al. (1993) is applicable. The algorithm was based on measurements made locally on the Greenland ice sheet and is therefore viewed as the most accurate method currently available for use with AVHRR thermal infrared data. Without other in situ surface temperature measurements for different elevation regions or for different seasons (e.g., during winter), it is impossible to derive an alternative model. The limitations due to varying atmospheric conditions and surface emissivity, along with errors due to undetected clouds, will be regarded as part of the data error, which is assessed by comparisons with in situ data.

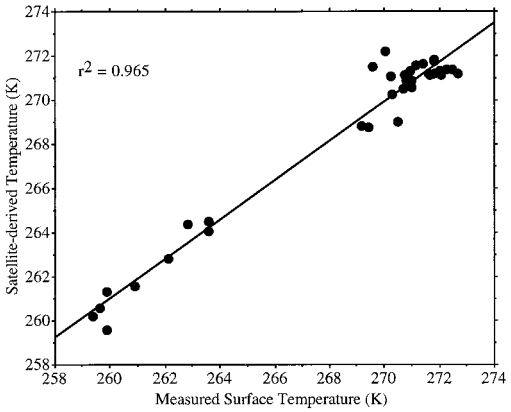

FIG. 3. Comparison between measured and satellite-derived surface temperatures during 1990 and 1991 at the ETH/CU camp. Data are for clear skies only. Regression of the data results in a line given by $y = 30.241 + 0.888x$, $r^2 = 0.966$, rms = 0.761 K.

3. Accuracy of the surface temperature

Surface temperatures were derived for each clear sky pixel from AVHRR GAC data during 1990 and 1991 when coincident surface temperature measurements were available from the ETH/CU camp. Surface temperatures were computed from the upwelling, broadband longwave radiation measured at the camp site using the following equation (Key et al. 1996):

$$T_{\text{surf}} = \left(\frac{L_{\text{up}} - (1 - \varepsilon) L_{\text{down}}}{\sigma \varepsilon} \right)^{0.25},$$

where L_{up} and L_{down} are the upwelling and downwelling longwave flux, respectively; σ is the Stefan–Boltzmann constant; and ε is the emissivity, assumed to be 0.99. Figure 3 compares the observed surface temperature and the satellite-derived surface temperature. Direct comparison gives good agreement for all temperatures with the largest differences found at 271 and 260 K. The mean difference between the in situ and calculated surface temperature is -0.065 K with a standard deviation of 0.899 K and a maximum temperature difference of 2.1 K. The differences between the means of the two measurements are not significant for a 99% confidence level.

The large discrepancies found at 271 and 260 K may be a result of clouds that went undetected and thus contaminated the camp pixel. The criteria used for flagging the camp pixel as cloudy is based on synoptic observations. Synoptic cloud observations during 1990 and 1991 are available at 3-h intervals only and do not coincide exactly with the time of the satellite overpass. At the higher temperatures, errors in surface temperature are also expected from comparing the satellite pixel (4 km) with a point measurement. During the summer months, melt occurs at the ETH/CU camp and surface lakes form near the camp. The occurrence of melt ponds and lakes will cause the satellite-derived temperatures to be lower. Due to the emissivity difference of dry/wet snow, the surface temperature retrieval has a bias of 0.3–0.5 K. This is observed in Fig. 3 where the surface-measured surface temperatures are slightly larger than those derived from AVHRR at temperatures around 273 K. Therefore, caution is needed in comparing the measurement at the camp with the larger area measured by the satellite during melt.

Some of the error in the calculated surface temperature is also a result of comparing measured surface temperature at half-hour intervals with instantaneous satellite measurements. Further, the previously mentioned uncertainties in atmospheric conditions and surface emissivity will add to the overall error.

Regression analysis of the data yields the following result:

$$T_s(\text{meas}) = 29.223 + 0.891 T_s(\text{calc}),$$

with a correlation coefficient of 0.965 and an rms error of 0.761 K. Here, T_s(meas) is the observed surface temperature and T_s(calc) is the surface temperature derived from AVHRR radiances. Hence, the AVHRR surface temperature data could be ''fine-tuned'' using the above equation. However, it is not known how representative the in situ data used in the analysis are for the entire ice sheet. There might be local effects, such as elevation changes, that need to be accounted for. In addition, snowmelt and melt ponding will alter the surface emissivity and the above equation would no longer be valid. These effects are difficult to assess without in situ surface temperature data from other locations.

For the above-stated reasons, no fine-tuning of the AVHRR-derived surface temperature is performed. It is estimated, however, that the average deviation of AVHRR surface temperatures from the ''true'' surface temperatures during summer is less than 1 K. Since the uncertainty of the surface radiation measurements is given as 3% (Haefliger et al. 1993), the error is within the uncertainty of the measurement.

4. Results

Figures 4a,b show the mean monthly surface temperature computed for January and July 1989. Remember that these are not true monthly means but the monthly mean at approximately 1500 GMT. The diurnal cycle of air temperature is largest in spring and fall ($T_{\text{max}} - T_{\text{min}} = 10$ K) and nonexistent during winter. In Figures 4a,b we observe the temperature gradually decreases with increasing elevation, and the minimum temperatures are found in the Summit region (Fig. 1). Thus, the ice sheet temperatures are dominated by elevation, with the temperature isotherms corresponding closely with the elevation contours.

Although the coldest areas are identified with the high-elevation region (Summit and South Dome areas), the coldest temperatures are not always located at the highest elevations. The location of the minimum tem-

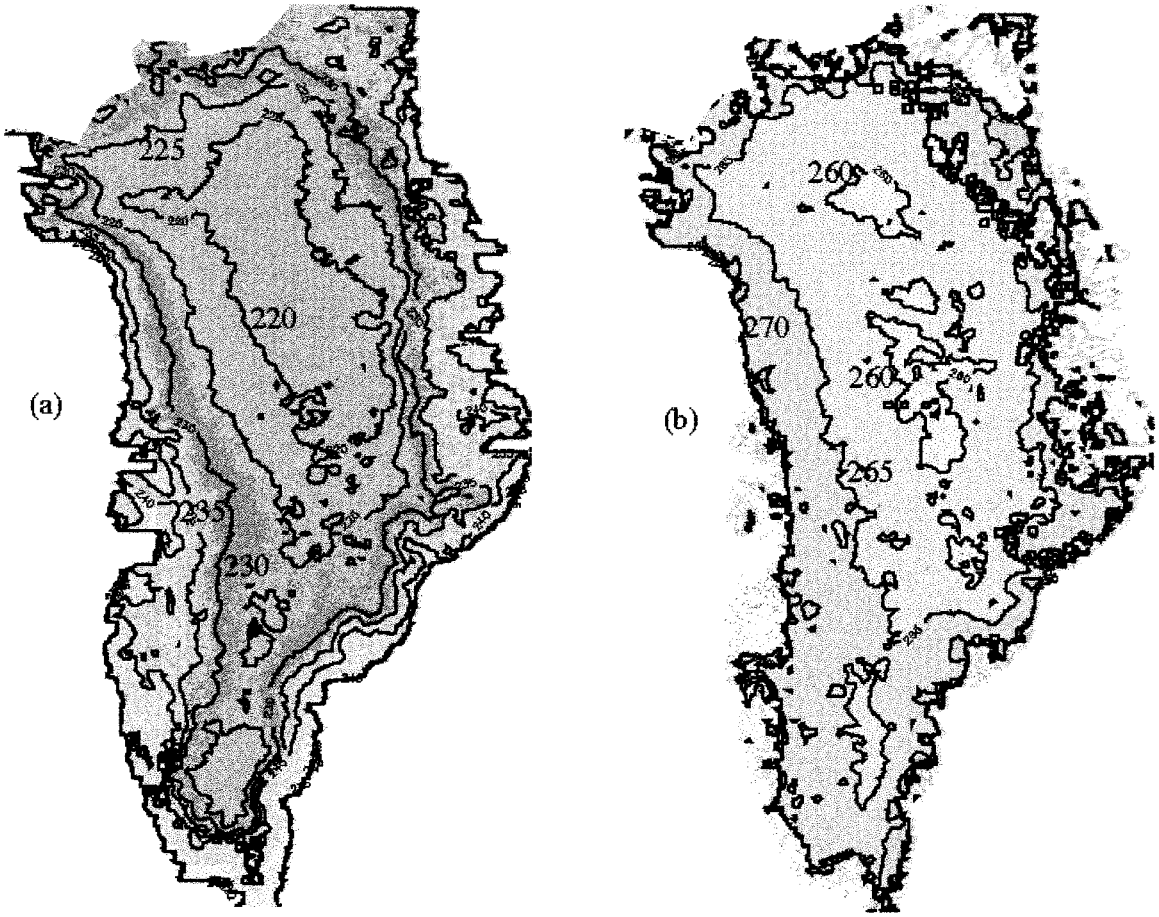

FIG. 4. Monthly surface temperature for the Greenland ice sheet during (a) January and (b) July 1989.

perature is found to move several hundred kilometers from month to month. In fact, during polar night the latitudinal effect seems to dominate as the minimum surface temperatures are found as far north as 76°N.

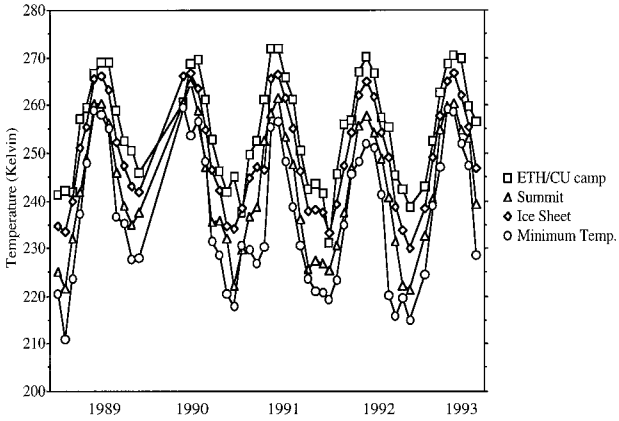

FIG. 5. Monthly surface temperatures at the ETH/CU camp, summit, and for the entire Greenland ice sheet (minimum and mean) from January 1989 through October 1993. Data are missing for January through May 1990.

The highest temperatures are found along the west coast and near the southern tip of Greenland. Along the southwestern part of the ice sheet, higher temperatures occur farther inland than on the eastern slope. This can be explained by the difference in elevation between the east and west coasts and the close proximity to open water along the western coast. During early spring, open water becomes apparent, and the North Water polynya expands considerably, joining up with open water areas to the south (Gloersen et al. 1992).

Figure 5 depicts the mean monthly surface temperatures at the ETH/CU camp, at the Summit, and average and minimum surface temperatures for the entire Greenland ice sheet from January 1989 through October 1993. Data are missing between January and May 1990. Seasonally, the monthly cloud-free surface temperatures vary by as much as 40°C. During the summer months, the highest temperatures occur in July, with the maximum temperatures found at the ETH/CU camp (~270 K). The ETH/CU camp is located at the equilibrium line altitude along the west coast of the ice sheet and tends to experience significant melt during the summer months. During summer melt, the surface albedo drops from values as high as 0.85 for dry snow to values as

low as 0.6, doubling the amount of solar energy absorbed by the snowpack and thereby increasing the snowpack temperature.

Snow does not melt at the Summit, where the summer surface temperatures are well below 273 K. Even though the temperatures remain below melting at the Summit, the contrast between the Summit and ETH/CU camp surface temperatures is smallest in summer. Figure 5 also indicates that the minimum ice sheet surface temperatures more closely match those found at the summit during summer, whereas during winter this is no longer the case. As mentioned previously, during polar night the lowest surface temperatures are farther north. The maximum surface temperature coincides with the largest sun angle, and it is interesting to note that the winter minimum surface temperature occurs almost symmetrically (e.g., 6 months before and after the maximum surface temperature).

Autumn brings increased cyclonic activity and snowfall. In the central part of the ice sheet (e.g., Summit), the temperatures fall more quickly than along the coast (e.g., ETH/CU camp) due to decreased incoming solar radiation. At the coast, proximity to open water delays the first cooling. Figure 5 also shows large interannual variability in the winter surface temperatures. The surface temperature variability in winter reflects the variability in storms. Large interdiurnal temperature changes on the ice sheet are frequently observed with the destruction, or building, of a surface inversion. During interstorm periods, extreme cooling of the snow surface results and a deep surface inversion forms. The typical scenario is that with decreasing wind speed, the surface temperature begins to drop and a surface inversion establishes itself due to radiative cooling of the surface. When a storm occurs (e.g., katabatic storms that are common along the perimeter of the ice sheet), temperatures at the snow surface rise as a result of turbulent mixing with the warmer air above (Miller 1956). During such periods, surface temperatures may rise by as much as 20° or more (Fig. 6). Higher temperatures are also usually accompanied by an increase in wind speed. The predominant wind on the ice sheet is katabatic.

Figures 7a–d depict the mean July surface temperatures from 1989 to 1993, excluding 1990. The lowest July surface temperatures in the time series were observed in 1992, with temperatures almost 2 K colder than the previous years. During 1993, the temperatures began to rise again but still remained less than those of the years prior to 1992. Passive microwave observations (Abdalati and Steffen 1997) also suggest a minimum melt extent for 1992. The temperature anomaly of 1992 could be explained by the Mount Pinatubo eruption and the subsequent release of optically active aerosols into the stratosphere (Minnus et al. 1993). The lower temperatures could also be attributed to the El Niño event of 1992. During the 1992 El Niño, surface air temperatures were found to be significantly lower over the

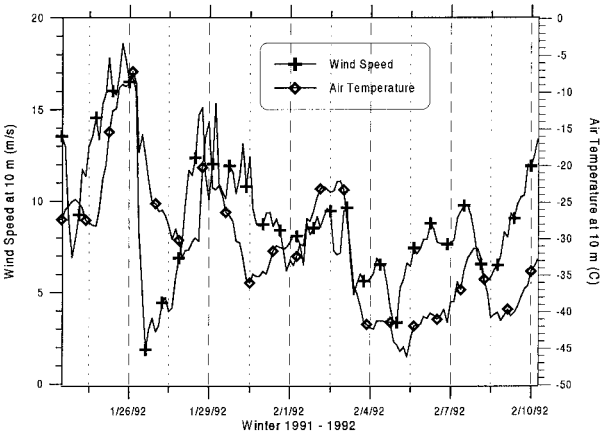

FIG. 6. Near-surface air temperature at the ETH/CU camp during January and February 1992. Strong temperature fluctuations (e.g., warming) are related to turbulent mixing of warmer air from the inversion height to the surface during katabatic storm events. The time lag between wind speed increase/decrease and surface temperature warming/cooling is approximately 10 h. For wind speed greater than 8 m s^{-1}, the correlation between surface air temperature and wind speed is $r = 0.84$ for a total of 75 3-h measurements during a 3-month period.

entire Northern Hemisphere land areas (Greenland was excluded from the analysis), associated with an increase in the Northern Hemisphere snow extent (Groisman et al. 1994).

The temperature seesaw and the associated North Atlantic Oscillation (NAO) also have an influence on temperatures over Greenland. During periods of intensification of the normal mode of the NAO (deep Icelandic low and a strengthened Azores high), mean monthly temperatures in Greenland are below normal (Barlow et al. 1993). The temperature seesaw is recorded in the GISP 2 (Greenland Ice Sheet Project 2) ice core isotopic signal and shows that although the temperature signal is strongest during winter, it is also apparent in summer (Barlow et al. 1993). Furthermore, the signal at the Summit camp site is in agreement with the long-term meteorological record at Jakobshavn, located on the west coast of Greenland (see Fig. 1). However, from 1989 through 1993 the NAO was positive for all 5 years (Hurrell 1995). Therefore, the anomalously lower temperatures during 1992 cannot be explained by variations in the NAO and temperature seesaw alone.

Finally, variations and trends in snow cover are known to be linked to the surface air temperature variations (Groisman et al. 1994). Similarly, the melt extent of the Greenland ice sheet is highly correlated with the coastal temperatures around Greenland (Abdalati and Steffen 1997). The increase in coastal surface temperature from 1979 to 1991 is reflected in an increase in melt extent on the Greenland ice sheet (Abdalati and Steffen 1997). From 1989 to 1991, AVHRR-derived surface temperatures also show a slight increase in the summer temperatures. In 1992, surface temperatures fall

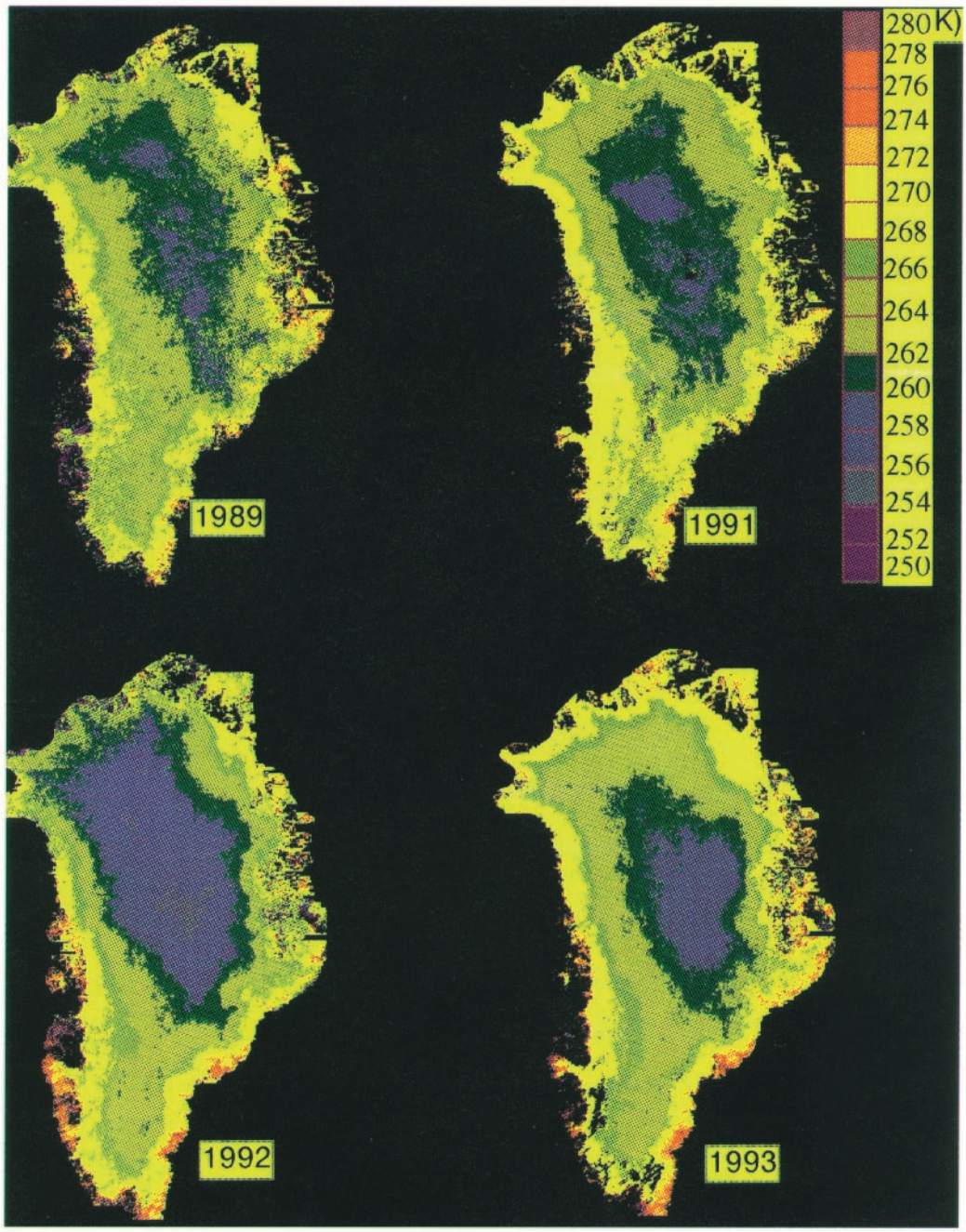

FIG. 7. AVHRR-derived surface temperature for 1989, 1991, 1992, and 1993 during July.

slightly and are consistent with a decrease in the melt on the Greenland ice sheet (Abdalati and Steffen 1997).

It is important to keep in mind, however, that the accuracy of the snow surface temperature retrieval algorithm of Haefliger et al. (1993) is degraded by the variability in atmospheric conditions. The split-window technique is particularly sensitive to changes in atmospheric conditions, such as the presence of volcanic aerosols in the stratosphere (Stroeve et al. 1996). Therefore, the quality of the 1992 satellite-derived surface temperatures may be in question. Unfortunately, we do not have any in situ measurements from 1992 with which to compare our results.

5. Conclusions

This article describes the spatial and temporal variability of clear-sky surface temperatures at 1500 GMT

over the Greenland ice sheet from 1989 through 1993. Surface temperatures are derived from AVHRR thermal radiances following the procedure outlined in Haefliger et al. (1993). During summer, the accuracy of dry snow surface temperature is estimated to be better than 1 K. In summer, minimum surface temperatures are found at the summit and maximum temperatures along the western coast and southern tip of the ice sheet. In winter, minimum surface temperatures are still found at high elevations but tend to migrate farther north.

Maximum surface temperatures occur in July when the amount of absorbed solar radiation at the surface reaches its maximum. No significant trend in surface temperature is observed for the 5 years analyzed. However, even though the interannual variability of summer surface temperature is small, 1992 shows a marked decrease in surface temperature compared with the other years. For example, in July, temperatures were almost 2° lower than in the other years. This is believed to be a consequence of the eruption of Mount Pinatubo during June 1991. The sensitivity of the split-window technique to stratospheric aerosols likely introduces an error to the satellite-derived surface temperatures during 1992. However, the lower surface temperatures are consistent with passive microwave observations during the same time.

It is also interesting to note that the summer temperatures were slightly higher in 1990 than the other years. This was also a year of minimum Northern Hemispheric sea ice extent (Serreze et al. 1995). Thus, the higher temperatures over Greenland during 1990 are consistent with those found elsewhere in the Arctic.

In winter, katabatic winds significantly modify the local climate through vertical mixing, and sudden large increases in surface temperature may occur, with temperatures reaching as high as 273 K. In the absence of strong winds, the surface temperature remains low, and large surface inversions are common over the ice sheet. The large interannual variations found in winter surface temperatures could also be an artifact of the cloud detection algorithm used. Cloud-masking during winter proved to be much more difficult due to the relatively low temperature contrasts between cloudy and clear sky conditions. Unfortunately, a reliable automated cloud-detection algorithm using AVHRR data in polar regions does not yet exist. Until we can accurately detect clouds over snow- and ice-covered surfaces, surface temperatures will likely be in error by 1–2 K, with the greatest errors in surface temperature occurring during polar night.

Acknowledgments. This work was supported under Contract NAGW-2158 by NASA Ocean Science Branch and the National Science Foundation OPP-9321547. AVHRR GAC data was provided by the National Center for Atmospheric Research.

REFERENCES

Abdalati, W., and K. Steffen, 1997: Snowmelt on the Greenland ice sheet as derived from passive microwave satellite data. *J. Climate,* **10,** 165–175.

Baldwin, D. G., and W. J. Emery, 1993: A systematized approach to AVHRR image navigation. *Ann. Glaciol.,* **17,** 414–420.

Barlow, L. K., J. W. C. White, R. G. Barry, J. C. Rogers, and P. M. Grootes, 1993: The North Atlantic Oscillation signature in deuterium and deuterium excess signals in the Greenland Ice Sheet Project 2 ice core, 1840–1970. *Geophys. Res. Lett.,* **20,** 2901–2904.

Dozier, J., and S. G. Warren, 1982: Effect of viewing angle on the infrared brightness temperature of snow. *Water Resour. Res.,* **18,** 1424–1434.

Gloersen, P., W. Campbell, D. Cavalieri, J. Comiso, C. Parkinson, and J. Zwally, 1992: Arctic and Antarctic sea ice, 1978–1987: Satellite passive-microwave observations and analysis. NASA SP-511, 290 pp.

Groisman, P. Y., T. R. Karl, and R. W. Knight, 1994: Changes of snow cover, temperature, and radiative heat balance over the Northern Hemisphere. *J. Climate,* **7,** 1633–1656.

Haefliger, M., K. Steffen, and C. Fowler, 1993: AVHRR surface temperature and narrow-band albedo comparison with ground measurements for the Greenland ice sheet. *Ann. Glaciol.,* **17,** 49–54.

Hurrell, J., 1995: Decadal trends in the North Atlantic Oscillation: Regional temperatures and precipitation. *Science,* **269,** 676–679.

Key, J., 1996: The Cloud and Surface Parameter Retrieval (CASPR) system user's guide. Dept. of Geography, Boston University, Tech. Rep. 96-02, 90 pp. [Available from Jeff Key, Dept. of Geography, Boston University, 675 Commonwealth Ave., Boston, MA 02215.]

——, and M. Haefliger, 1992: Arctic ice surface temperature retrieval from AVHRR thermal channels. *J. Geophys. Res.,* **97,** 5885–5893.

——, J. Collins, C. Fowler, and R. Stone, 1996: High-latitude surface temperature estimates from thermal satellite data. *Remote Sens. Environ.,* in press.

Kidwell, K. B., 1991: NOAA polar orbiter data users guide. NOAA Information Service and Climate Data Center, Satellite Data Service Division, Washington, DC, 204 pp. [Available from NCDC, World Weather Building, Rm. 100, Washington, DC 20233.]

Lindsay, R. W., and D. A. Rothrock, 1994: Arctic sea ice surface temperature from AVHRR. *J. Climate,* **7,** 174–183.

McClain, E. P., W. G. Pichel, and C. C. Walton, 1985: Comparative performance of AVHRR-based multichannel sea surface temperatures. *J. Geophys. Res.,* **90,** 11 587–11 601.

McMillin, L. M., 1975: Estimation of sea surface temperatures from two infrared window measurements with different absorption. *J. Geophys. Res.,* **80,** 5113–5117.

Miller, D. H., 1956: The influence of snow cover on local climate in Greenland. *J. Meteor.,* **13,** 112–120.

Minnus, P., E. F. Harrison, L. L. Stowe, G. G. Gibson, F. M. Denn, D. R. Doelling, and W. L. Smith Jr., 1993: Radiative climate forcing by the Mount Pinatubo eruption. *Science,* **259,** 1411–1415.

Price, J. C., 1983: Estimating surface temperature from satellite thermal infrared data—A simple formulation for the atmospheric effect. *Remote Sens. Environ.,* **13,** 353–361.

Rao, C. R. N., 1993: Nonlinearity corrections for the thermal infrared channels of the Advanced Very High Resolution Radiometer: Assessment and recommendations. NOAA Tech. Rep. NESDIS-69, NOAA/NESDIS, Washington, DC, 31 pp. [Available from NOAA/NESDIS Satellite Research Laboratory, Washington, DC 20233.]

Raschke, E., P. Bauer, and H. J. Lutz, 1992: Remote sensing of clouds and surface radiation budget over polar regions. *Int. J. Remote Sens.,* **13,** 13–22.

Salisbury, J. W., D. M. D'Aria, and A. Wald, 1994: Measurements

of thermal infrared spectral reflectance of frost, snow, and ice. *J. Geophys. Res.,* **99,** 24 235–24 240.

Serreze, M., J. Maslanik, J. Key, and R. Kokaly, 1995: Diagnosis of the record minimum in Arctic sea ice area during 1990 and associated snow cover extremes. *Geophys. Res. Lett.,* **22,** 2183–2186.

Steffen, K., 1995: AVHRR applications for ice surface studies. *Oceanographic Applications of Remote Sensing*, M. Ikeda and F. W. Dobson, Eds., CRC Press, 307–320.

——, W. Abdalati, and J. Stroeve, 1993: Climate sensitivity studies of the Greenland ice sheet using satellite AVHRR, SMMR, SSM/I, and in situ data. *Meteor. Atmos. Phys.,* **51,** 239–258.

Stroeve, J., M. Haefliger, and K. Steffen, 1996: Surface temperature from *ERS-1* ATSR infrared thermal satellite data in polar regions. *J. Appl. Meteor.,* **35,** 1231–1239.

Wald, A., 1994: Modeling thermal infrared (2–14 μm) reflectance spectra of frost and snow. *J. Geophys. Res.,* **99,** 24 241–24 250.

Yamanouchi, T., and S. Kawaguchi, 1992: Cloud distribution in the Antarctic from AVHRR data and radiation measurements at the surface. *Int. J. Remote Sens.,* **13,** 111–127.